Progress of the Recent Experimental Research on the J-TEXT Tokamak

G. Zhuang[1], K.W. Gentle[2], Z.Y. Chen[1], Z.P. Chen[1], Z.J. Yang[1], Wei Zheng[1], Q.M. Hu[1], J. Chen[1], B. Rao[1], W.L. Zhong[3], K.J. Zhao[3], L. Gao[1], Z.F. Cheng[1], X.Q. Zhang[1], L. Wang[1], Z.H. Jiang[1], T. Xu[1], M. Zhang[1], Z.J. Wang[1], Y.H. Ding[1], K.X. Yu[1], X.W. Hu[1], Y. Pan[1], H. Huang[2], the J-TEXT team[1]

[1]State Key Laboratory of Advanced Electromagnetic Engineering and Technology, School of Electrical and Electronic Engineering, Huazhong University of Science and Technology, Wuhan Hubei, 430074, China

[2]Institute for Fusion Studies, University of Texas at Austin, Austin, 78712, USA

[3]Southwestern Institute of Physics, Chengdu Sichuan, China

E-mail contact of main author: ge-zhuang@mail.hust.edu.cn

Abstract. The progress of experimental research over last two years on the J-TEXT tokamak is reviewed and reported in this paper, and include: investigations of resonant magnetic perturbations (RMPs) on the J-TEXT operation region show that moderate amplitude of applied RMPs either increases the density limit from less than $0.7n_G$ to $0.85n_G$ (n_G is the Greenwald density, $n_G = I_p/\pi a^2$) or lowers edge safety factor q_a from 2.15 to nearly 2.0; experimental results in the high-density disruption plasmas confirm that local current shrinkage during a multifaceted asymmetric radiation from the edge can directly terminate the discharge; observations of influence of RMPs with a large m/n = 3/1 dominant component (where m and n are the toroidal and ploloidal mode number, respectively) on electron density indicate electron density first increases (decreases) inside (around/outside) of the 3/1 rational surface, and it is increased globally later together with enhanced edge recycling; measurements by a multi-channel Doppler reflectometer show that the quasi-coherent modes in the electron diamagnetic direction occur in the J-TEXT ohmic confinement regime in a large plasma region (r/a ~ 0.3 − 0.8) with frequency of 30 – 140 kHz; investigations of the RMPs on the behavior of runaway electrons/current show that application of the RMPs with m/n=2/1 dominant component during disruptions can reduce runaway production and furthermore, its application before the disruption can reduce both the amplitude and the length of runaway current; etc.

1. Introduction

The Joint-Texas EXperimental Tokamak (J-TEXT) has a major radius R_0 = 105 cm and a minor radius a = 25-29 cm with a movable titanium-carbide coated graphite limiter [1]. Nowadays the typical J-TEXT discharge in the limiter configuration is done with center-line toroidal field B_t of ~2.0 T, plasma current I_p of ~200 kA lasting for 400 ms, plasma densities n_e of $1\sim7\times10^{19}$ m^{-3}, and electron temperature T_e of ~1 keV [2]. Over last two years, there has been significant progress in J-TEXT experimental research including: investigation of the effect of resonant magnetic perturbations (RMPs) on the J-TEXT operation region and understanding of multifaceted asymmetric radiation from the edge (dubbed a "MARFE") as a cause of the density limit; study of the effect of RMPs on particle transport and identification of the quasi-coherent characteristics in spectra of density fluctuations; observations of behavior of runaway current by RMPs, and so on.

On J-TEXT, there are two sets of RMP coil system [3]: One can generate a static helical field perturbation (usually named static RMPs) with a m/n = 2/1 or 3/1 dominant component, where m and n are the poloidal and toroidal mode number, respectively; the other can generate either a rotating or static helical field perturbation with a maximum rotation frequency up to 10 kHz and dominant resonant modes of m/n = 2/1, 3/1 or 1/1. Previous studies [3, 4-7] of RMP influences on a tokamak plasma revealed that the applied RMPs contribute a net stabilizing and braking effect on the tearing mode (TM) and plasma rotation. Further numerical modeling shows that a smaller amplitude of TM can be suppressed more easily by RMPs [6], suggesting that it is possible to take the advantage of RMPs to control the precursor TM for disruption mitigation. With this motivation, experiments on J-TEXT in an attempt to study the RMPs effect on high density limit and low-q limit discharges and thus, to extend the operating regime, are carried out. The limitation of the operating regime due to the high density MARFE associated with the plasma density limit [8-10] has been observed on many tokamaks. The development of MARFEs tends to disrupt the plasma current at very high densities, but its origin remains unclear. Since plasma operation in future fusion reactors relies on high density operation to achieve maximum fusion performance, the understanding of the physical mechanism of disruptions due to MARFE occurrence is of extreme importance. The investigation of high density plasmas characterized by MARFEs has been conducted on the J-TEXT.

J-TEXT has a long-term interests and makes continuous efforts to investigate transport and turbulence in tokamak plasmas. Over the last two years, J-TEXT focused on the influence of MHD activity on particle transport. In order to carry out this investigation, the RMPs with a large 3/1 dominant component were applied to a plasma to observe the density response. Apart from the particle transport, the momentum transport is also studied by using biasing electrodes on the J-TEXT. Turbulent transport is also a main topic of J-TEXT experimental research. The turbulent transport is mainly attributed to two types of electrostatic turbulence: ion temperature gradient (ITG) modes and trapped electron modes (TEM). Theoretical work has predicted that they can be driven unstable in core plasma at long wavelength scale, and their excitation thresholds strongly depend on density and temperature gradients [11, 12]. Experimentally, it is challenging to directly discriminate them by scale-resolved measurement since they usually coexist and their wavelengths overlap each other. Studying the effects of them on plasma transport provides an alternative way to indirectly discriminate them. For instance, the observation of critical gradients for both heat and particle transport has revealed the excitation of ITG or TEM [13-17]. In recent years, more attention has been paid to discriminating TEM and ITG from fluctuation spectra [16, 18-20]. By using multi-channel Doppler reflectometer, a fine-scale study of electrostatic turbulence structure may be possible.

The potential damage due to large runaway current generated by disruptions remains a serious problem for next generation devices. There are, generally, three mechanisms for RE generation: primary generation (Dreicer generation), secondary generation (avalanche generation) and hot tail generation [21]. The high electric fields induced during the current quench phase of a tokamak disruption can generate a large number of REs. For example, the generation of a 10 MA RE beam with energies of several tens of MeV would be possible when a disruption in a machine, like ITER occurs. Consequently, it could damage the vacuum vessel and the structures of the machine. Therefore the suppression of runaway generation during disruption is necessary. The potential scenario of the application of RMP during a disruption aiming to suppress the runaway electrons has been proposed, and attempts have been made on JT-60U [22, 23], TEXTOR [24, 25] and JET. The results seem different. Motivated by further understanding of the suppression effect of RMP on runaway production, the application of RMP during a plasma disruption was carried out on a small scale machine, J-TEXT.

The remainder of the paper is organized as follows: In Section 2, the extension of the J-TEXT operating regime by RMPs and investigation of the density limitation are described; In Section 3, the experimental studies of particle transport, momentum transport and turbulent transport on J-TEXT are surveyed; in Section 4, the suppression of runaway current by RMPs is delineated. The last section offers conclusions.

2. Explorations of the Operation Regime and Comprehension of Density Limit

2.1. Effect of RMPs on Disruption Limit

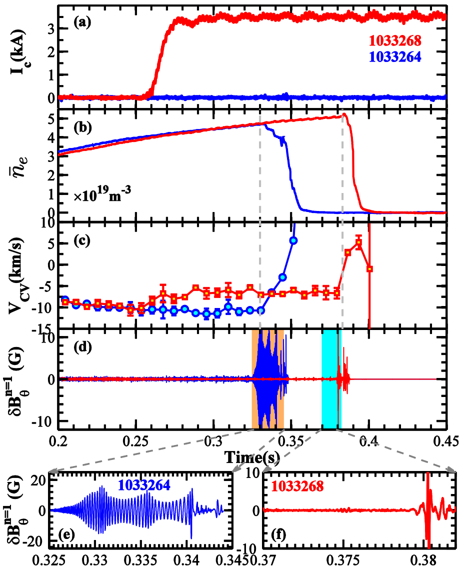

FIG. 1. Influence of static RMP on density limit. Time traces of (a) static RMPs current I_c, (b) line-averaged electron density $\bar{n}_e$, (c) plasma toroidal rotation of CV impurity V_{CV}, (d) n = 1 magnetic perturbation $\delta B_\theta^{n=1}$ for shots 1033264 and 1033268, and detail evolution of $\delta B_\theta^{n=1}$ for shot (e) 1033264 and (f) 1033268.

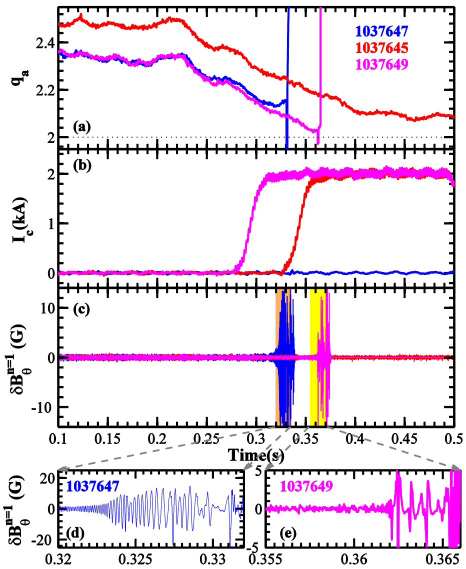

FIG. 2. Influence of static RMP on low-q discharge. Time traces of (a) edge safety factor q_a, (b) static RMP current I_c, (c) n = 1 magnetic perturbation $\delta B_\theta^{n=1}$ for shots 1037647, 1037645 and 1037649, and detail evolution of $\delta B_\theta^{n=1}$ for shot (d) 1037647 and (e) 1037649.

On J-TEXT, an m/n = 2/1 TM grows quickly when approaching the high density or low-q limit, and it rotates in the counter-I_p direction with a frequency decreasing from 10 kHz to 2 kHz as shown in Fig. 1 for shot 1033264. For shot 1033264, the density limit is $n_e = 4.7 \times 10^{19}$ $m^{-3} = 0.68\ n_G$ (n_G is the Greenwald density, $n_G = I_p/\pi a^2$). For comparison, the static RMPs are applied for shot 1033268 before the onset of the precursor TM, as shown in the same figure. The static RMP coil current (I_c) is turned on at t = 0.26 s, then ramped up to 3.5 kA in 0.02s for shot 1033268 (Fig. 1(a)). During the application of a weaker static RMP, the core line-averaged electron density increases to 5.25×10^{19} $m^{-3} = 0.77 n_G$, and then a disruption happens at t = 0.38s. When looking into the time evolution of $\delta B_\theta^{n=1}$ in Figs. 1(d) and 1(f), it is found that there is no precursor TM until disruption, indicating that it is completely suppressed. In addition, the toroidal rotation V_{CV} measured by visible spectrum edge rotation diagnostic (ERD) [26] decreases slightly from -10.1 km/s to -7.2 km/s before disruption. Compared to the case without RMPs (shot 1033264), the density limit is increased by 12%.

Similar to the results shown in Fig. 1, the static RMPs are also applied in the low-q discharges. In order to approach the low-q limit, the plasma current is ramped up slowly after reaching its first flattop, the precursor 2/1 TM is often observed in low-q limit disruption, and the limit q_a is found to be around 2.2, as shown in Fig. 2 for shot 1037647. Fig. 2 also gives the effect of static RMPs on low-q discharges for shots 1037645 and 1037649. The static RMP is applied when q_a decreases to 2.2 with I_c = 2 kA at the flattop. Compared to the case without RMPs (shot 1037647), disruption does not occur for shot 1037645 with a lower q_a, q_a = 2.1. For shot 1037649, disruption happens as q_a approaching 2.0. The evolution of $\delta B_\theta^{n=1}$ just before disruption shown in Figs. 2(c) and 2(e) reveals that the precursor TM is also completely suppressed. The results shown in Fig. 2 reveal that static RMPs can lower the low-q limit from 2.15 to 2 and suppress the precursor TM. Additional studies have also been carried out to look into the effect of RMP amplitude: it is found that lowest q_a, q_a = 2 is approached for 1 kA ≤ I_c ≤ 2.5 kA, while stronger RMPs trigger the disruption at higher q_a. However, the q_a = 2 limit has never been overcome.

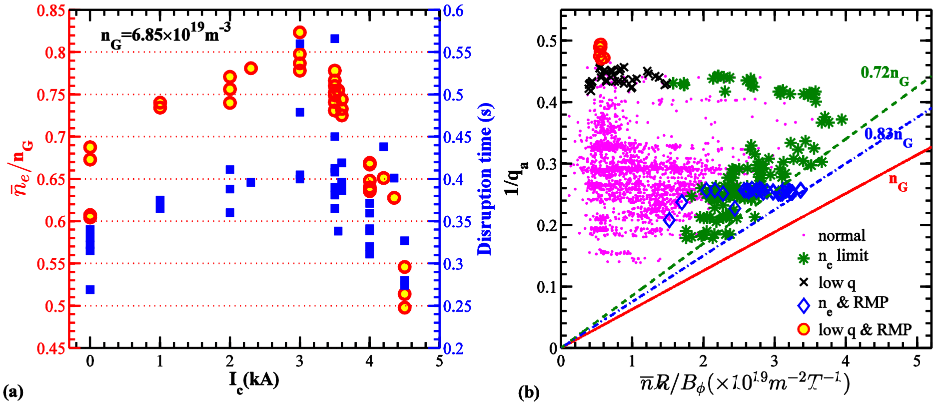

FIG. 3. (a) Ratio between n_e and Greenwald density n_G (red circles) and the disruption time (blue squares) versus static RMPs current I_c. (b) The J-TEXT operating region (Hugill diagrams) with graphite in 2014 and 2015. The magenta solid points (•), the green asterisks (*) and the black cross (×) represent the normal stable discharges without disruptions the density limit disruptions and the low-q disruptions, respectively. The blue diamonds (◊) and the red circles (o) represent the density limit and low-q limit discharges with application of RMPs, respectively. The red solid line marked with n_G indicates the Greenwald density limit.

Corresponding to Fig. 1, systematic experiments have been carried out by keeping the background plasma parameters the same, while only the amplitude of static RMPs are changed by scanning I_c from 1 kA to 4.5 kA. In Fig. 3(a), n_e/n_G and the disruption time are shown as a function of I_c. The density is usually limited to $n_e < 0.68n_G$ and disruption happens at t < 0.33 s without the application of static RMPs. The density limit linearly increases with I_c for I_c ≤ 3 kA. Static RMPs increase the density limit to more than $0.8n_G$ for I_c = 3 kA. However, even stronger RMPs do not lead to a further increase in the limit density but a decrease in it with an earlier disruption. The density limit decreases from about ~$0.8n_G$ to $0.5n_G$ when I_c increases from 3 kA to 4.5 kA. Results shown in Figs. 1 to 3(a) indicate that the applied static RMPs partially expand the plasma parameters, which is shown in Fig. 3(b) by plotting the inverse edge safety factor $1/q_a$ against the Murakami parameter (or normalized density)n_eR/B_t.

The investigations verify that the density limit can increase from less than $0.7n_G$ to $0.85n_G$ and edge safety factor q_a drop from 2.15 to nearly 2.0 by applying the RMPs appropriately.

2.2. Local Current Shrinkage during a Multifaceted Asymmetric Radiation from the Edge

The experimental observations of high-density discharges on J-TEXT confirm that the discharges characterized by MARFEs always disrupt as the plasma density approaches an upper limit and they have almost identical performance. Here the plasma density and current density profiles are provided by a newly developed 17-channel far infrared polarimeter-interferometer (POLARIS) [27, 28], which views the plasma vertically at x = -24, -21, -18, -

15, -12, -9, -6, -3, 0, 3, 6, 9, 12, 15, 18, 21, 24 cm, where $x = R-R_0$. Here, $x < 0$ and $x > 0$ correspond to HFS and low field side (LFS), respectively. A typical high-density disruption discharge (shot #1038116) is shown in Fig. 4. The plasma parameters are I_p = 170 kA, B_t = 2.1 T, a = 0.255 m, and the edge safety factor q_a = 3.85. The discharge is terminated at t = 0.42 s and the maximum central line-averaged density is 5.6×10^{19} m^{-3} = 0.67 n_G. During 0.2 s < t < 0.4 s, the central (at x = 0 cm) line-averaged electron density $n_e(0)$ keeps increasing (Fig. 4(a)) and n_e at x = -24 cm (very edge of HFS) suddenly surges upward at about t = 0.33 s while it changes little or even drops at x = 24 cm (very edge of LFS) as shown in (Fig. 4(b)), implying an asymmetry in density profile occurs between the very edge of LFS and HFS.

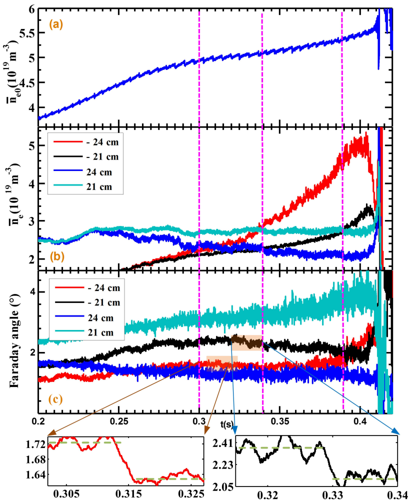

FIG. 4. A typical density limit disruption discharge. (a) central line-averaged density measured by FIR polarimeter-interferometer, (b) the 4-channel line-averaged density at the edge of plasma, (c) the 4-channel line-integral Faraday angle at the edge of LFS and HFS.

Correspondingly, the Faraday rotation angle at x = -24 cm (Fig. 4(c)) drops clearly at t = 0.315 s but no evident change at LFS. Similar behaviors also appear for the Faraday rotation angle at x = -21 cm. The Faraday rotation angle is described as $\alpha \sim \int n_e B_{\parallel} dZ$, where n_e is the electron density, $B_{\parallel}$ is the magnetic field parallel to the probing laser beam, $B_{\parallel} = B_\theta \cos\theta$, and θ is the angle between the probing beam and poloidal magnetic field B_θ. It is reasonable to infer that the decrease in Faraday rotation angle is caused by a rapid change of B_θ, which arises from a rapid change of local current density.

In Fig. 5(a), the visible CCD camera records a bright blob at the edge of the HFS: here three time points t = 0.30s, 0.34s, and 0.39s are shown to illustrate the evolution of the asymmetrical behaviors on the radial profile of electron density n_e (Fig. 5(b)) measured by the POLARIS, total radiation power P_{tot} (Fig. 5(c)) by the AXUV measurement, and poloidal magnetic field B_θ (Fig. 5(d)) measured by the POLARIS at the mid-plane Z = 0. It is found that a bright blob appears located outside the plasma at t = 0.30 s. As time evolves, the blob gets brighter and moves into the edge region of the plasma for t = 0.34 s, and the asymmetry in the profiles of n_e and B_θ are enhanced. Afterwards, the bright blob stays inside the plasma edge region for a few tens milliseconds, then it gradually rotates poloidally at t = 0.39 s and the discharge is terminated by a disruption at t = 0.41 s. All these characteristics of the diagnostic signals are referenced to the MARFE, The variation of poloidal magnetic field explains the sudden decreasing of Faraday rotation angle in Fig. 4. It is reasonably inferred that the plasma current density decreases while the electron density increases in the MARFE affected region. It should be noted that such disruptions are not caused by radiation collapse, since the total radiation power is only 30-40 percent of the Ohmic heating power, as shown in fig. 5(c). Some devices have already reported that the radiation collapse is not inevitable for density limit disruption discharges [29-31].

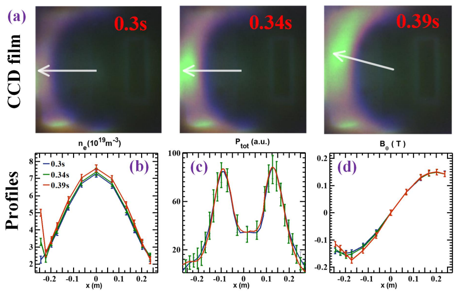

FIG. 5. Time evolution of (a) CCD records, and (b) electron density profiles, and (c) total radiation power profiles measured by AXUV, and (d) poloidal magnetic field profiles from the POLARIS data by use of tomographic inversion.

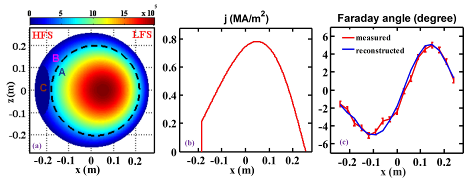

FIG. 6. (a) The constructed plasma current distribution, (b) the plasma current profile at the midplane, (c) the measured and calculated faraday angle.

A new interpretation for the J-TEXT MARFE is proposed based on the experimental observations. The increasing electron density in the MARFE region causes the local electron temperature to decrease to maintain the equilibrium, resulting in the increase of local resistance. The bright blob suggests that a population of neutral particles stays at the MARFE affected region. Both effects imply that the plasma current in the MARFE region may vanish or become very small, being consistent with the observation of the B_θ change shown in Fig. 5(d). To simplify, assume that the plasma current in the MARFE region is zero. The MARFE region is assumed to be an ellipse with 7cm width and 18cm height based on the observations of POLARIS, AXUV, and visible light CCD records, as marked as Region C in Fig. 6(a), where Region A is the innermost region with symmetric distribution of plasma current, Region B marks the region where the magnetic field lines terminate at the edge of MARFE area (similar to a 'limiter' [32]). With this assumption, the distribution of plasma current density can be reconstructed by implementation of equilibrium reconstruction techniques [33] based on the measured POLARIS data, as shown in Fig. 6(b). Thus the radial profiles of Faraday rotation angle can be calculated and given together with the measured results in Fig. 6(c). It is clear that the calculated Faraday rotation angle is in good agreement with the POLARIS measurements, indicating that localized plasma current shrinkage at the MARFE region is very pronounced and reasonable. As a consequence of the localized plasma current shrinkage in the MARFE region, the radial magnetic field is no longer zero in the plasma. When the asymmetry expands into the inner region, the magnitude of the radial magnetic field becomes considerably larger and much closer to the q = 2 rational surface, later on it is sufficient to trigger a locked mode, and a major disruption happens.

3. Survey on Experimental Research on Transport and Turbulence

3.1. Effect of RMPs on electron density

On J-TEXT, the influence of RMPs with a large m/n = 3/1 dominant component on electron density is studied [34]. An example of the effect of static 3/1 RMPs on the electron density during field penetration is shown in Fig. 7 for shot 1035319. Here I_p = 160 kA, B_t = 1.65 T, and q_a = 3.3. The central plasma rotation is observed to be in the electron diamagnetic drift direction, and the plasma is originally tearing stable. Before the application of RMPs, the plasma parameters remain nearly constant. The RMP coil current (I_c) is applied at 0.32 s (Fig. 7(a)), and it ramps up to the flattop of 6 kA at 0.36 s. Field penetration happens at t = 0.368 s as indicated by the fast growth of the locked mode detector signal b_r (red curve in Fig. 7(a)) when I_c ramps up to 5.9 kA. After field penetration, the line-integrated electron density n_eL at

R = 1.06 m begins to increase from 0.67×10^{19} m^{-2} to 0.75×10^{19} m^{-2} (Fig. 7(b)), with a relative change of 12%. At the same time, the electron temperature decreases slightly close to plasma core (R = 0.97 m) and more obvious at plasma edge (R = 0.85 m) as shown in Fig. 7(d). The soft X-ray emission (SXR) at plasma core increases and the effective Z_{eff} is slightly decreased (Fig. 7(c)). The edge recycling increases slightly as indicated by the Hα signal at r = 0.27 m. At t = 0.425 s mode unlocking happens when Ic ramps down to 4 kA, and all the parameters begin to recover to their initial values. The unlocking threshold is only one third smaller than the penetration threshold, being smaller than that for the 2/1 and other modes as reported on COMPASS [35], J-TEXT [6] and EXTRAP-T2R [36]. In Fig. 8, the time evolution of neL around the 3/1 rational surface (RS) at both LFS and HFS are shown. For shot 1035319 the 3/1 RS is found to be around R = 1.27 m at LFS and 0.9 m at HFS. It is found that n_eL first decreases quickly around/outside of the 3/1 RS (for R = 1.29 m at LFS and R ≤ 0.9 m at HFS) right after field penetration. Afterwards the n_eL increases both outside and inside the 3/1 RS.

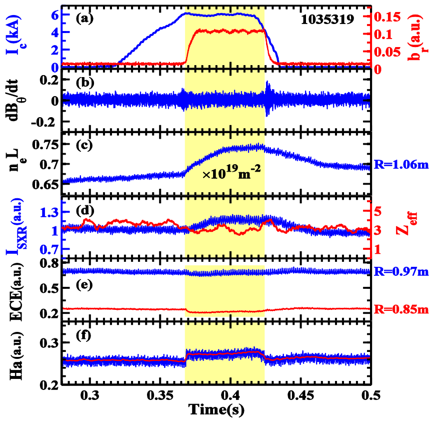

FIG. 7. Shot 1035319, penetration of static 3/1 RMPs. Time evolution of (a) I_c and b_r, (b) Mirnov signal dB_θ/dt, (c) core integrated density n_eL, (d) core SXR radiation intensity ISXR and Z_{eff}, (e) ECE signal at R = 0.97 m and 0.85 m, and (f) edge Hα signal.

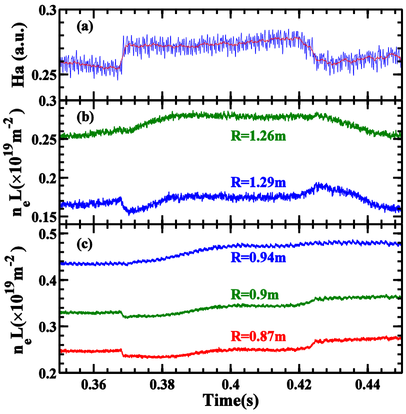

FIG. 8. Corresponding to figure 7, time evolution of (a) Hα signal, integrated electron density at (b) LFS (R = 1.26 m and 1.29 m) and (c) HFS (R = 0.87 m, 0.9 m, and 0.94 m).

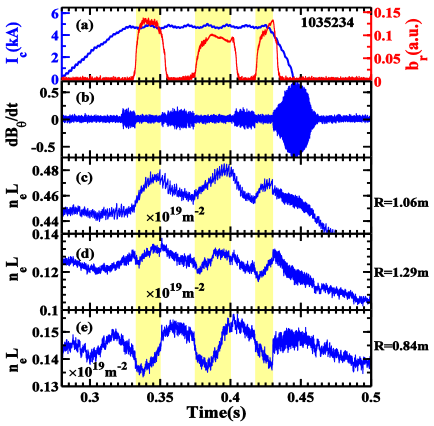

FIG. 9. Shot 1035234, penetration of static 3/1 RMPs. Time evolution of I_c, b_r, dB_θ/dt, integrated density n_eL at R = 1.06 m, 1.29 m and 0.84 m.

After field penetration, the increased density may exceed the density threshold for penetration and then force the locked mode to unlock when the amplitude of RMPs is not strong enough. One typical result is shown in Fig. 9 for shot 1035234, here I_c = 4.7 kA at the flattop and n_eL is 0.45×10^{19} m^{-2} before penetration. After field penetration at t = 0.33 s, edge n_eL decreases (at R = 1.29 m and 0.84 m) first, and later on it increases accompanying the increase of central density (n_eL at R = 1.06 m). At t = 0.35 s, the central n_eL increases to 0.48×10^{19} m^{-2} and the edge density exceeds the density threshold for penetration, so that mode unlocking happens spontaneously. The global density decreases after mode unlocking, which is similar to the result as shown in Fig. 7. When the density decreases to the value near the density threshold, field penetration happens again at t = 0.365 s and 0.42 s, respectively.

3.2.Perturbation on Toroidal Momentum Transport Due to Electrode Biasing

In the edge region of the J-TEXT, the electrode biasing (EB), which can yield a torque [37] of the same order of magnitude as a neutral beam torque, is applied to modulate the toroidal rotation. Thus, the toroidal momentum transport can be studied based on the perturbative analysis technique (PAT) [38]. The time traces of EB current (I_{EB}), central line averaged electron density ($\bar{n}_{e0}$) and impurity rotation speed (V_t at r/a = 0.56 ~ 0.82, C^{+4}) measured by ERD for a typical discharge (#1039782) with the EB modulation located at r/a ~ 0.9 are shown in Fig. 10. Here impurity rotation speed (V_t) is characterized as the toroidal plasma rotation. The modulated amplitude (δV_t) and phase delay (ϕ) can be extracted from a simple sinusoidal fitting. As the results, the profiles of electron density (n_e), rotation equilibrium V_{t0}, δV_t and ϕ are shown in Fig.11, respectively. With these profiles and a boundary condition which is defined as the core rotation velocity (r/a = 0~0.2) (Ar^{+16}) measured by x-ray imaging crystal spectrometer [39], the radial profiles of toroidal momentum transport coefficients (diffusivity χ_ϕ and convective velocity V_{conv}) of local plasma (normalized minor radius ϱ = 0.68–0.9) are also evaluated based on the PAT, as given in Fig. 12. The results indicate that χ_ϕ is in the range of 0 ~ 25 m^2s^{-1} and V_{conv} is about -30 ~ 0 ms^{-1}, representing a pinch effect in the momentum transport.

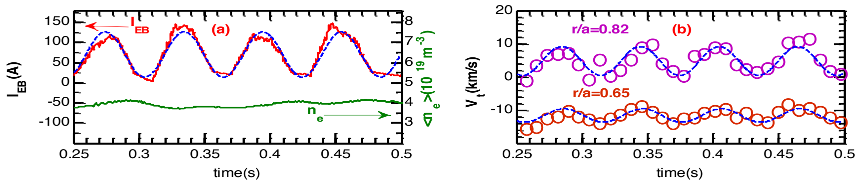

FIG. 10. Time evolutions of (a) EB current (I_{EB}) and central line averaged electron density ($\bar{n}_{e0}$) and (b) toroidal rotation at r/a = 0.82, 0.65 for a typical shot 1039782 with the EB modulation at r/a ~0.9. Blue lines are the sinusoidal fitting results

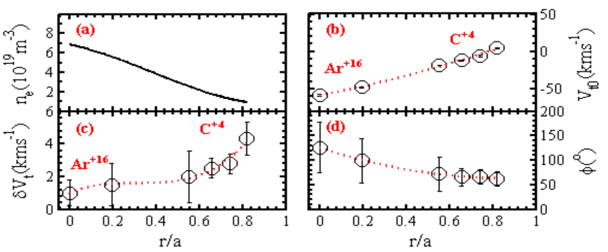

FIG. 11. Profiles of (a) electron density (n_e), (b) equilibrium of the toroidal rotation (V_{t0}), (c) the amplitude (δV_t) and (d) phase delay (ϕ) of the modulated toroidal rotation.

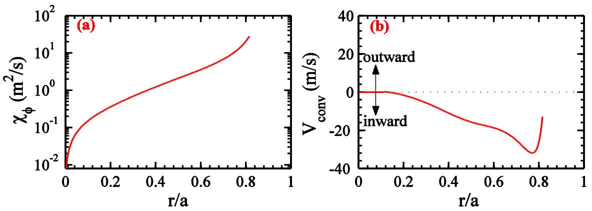

FIG. 12. Profiles of the toroidal momentum transport coefficients: (a) the diffusivity χ_ϕ and (b) the convection velocity V_{conv} in r/a = 0~0.82

3.3.Quasi-Coherent TEM in Density Fluctuation Spectra

To characterize the turbulence spectrum, K and Ka band multi-channel microwave reflectometers are used to measure the density fluctuations with radial resolution [40]. The ordinary mode (O-mode) polarization was set for these two systems. The corresponding electron densities at the cut-off layers are in the range of $0.4\text{-}1.8\times10^{19}$ m^{-3}. The systems acted as Doppler reflectometer by artificially introducing an incident angle between the microwave beam and the normal of the cut-off layer. They can measure both the density fluctuations and the perpendicular velocity of turbulence simultaneously. When the phase modulation is due to the cut-off (reflecting) layer oscillation caused by plasma instabilities, such as coherent or quasi-coherent mode, the characteristic frequency spectrum of the instability should be symmetric relative to f = 0. Fig. 13(a) is a typical frequency spectrum with a QC-TEM measured by Doppler reflectometry. The mode has intermediate frequency width (δf ~ tens of kHz) centered at a given frequency compared to that of coherent mode and broad-band turbulence. Here I_p = 180 kA, B_t = 2.0 T. The line-averaged electron density is 2.0×10^{19} m^{-3} and it is lower than the Shimomura density which was empirically predicted as the critical plasma density of the transition from linear ohmic confinement (LOC) to saturated ohmic confinement (SOC) regimes. When the line-averaged electron density (3.3×10^{19} m^{-3}) is higher than the Shimomura density, the QC-TEM is replaced by a broad-band spectrum as shown in Fig. 13(b). Nonlinear simulations have predicted that the ITG turbulence induces fluctuations with a broad-band frequency spectrum, whereas TEM generates a noticeable peak spectrum which is consistent with the observed QC-TEM [41]. The results indicate that the occurrence of TEM strongly depends on the plasma confinement regime. The radial features of QC-TEM can be obtained by multi-channel Doppler reflectometers. The central frequencies are in the range of 60-130 kHz as shown in Fig. 13(c). The measurement locations are in the core and edge region (r/a~ 0.3-0.8), where the mode frequency f_m increases with the cut-off density ($n_{e.c.}$), meaning f_m decreases with plasma minor radius. It is consistent with the observation in HL-2A. The critical gradients in heat and particle transport have been observed. It is worth directly studying the critical gradient for TEM excitation. The results from J-TEXT are shown in Fig. 13(d). The density peaking factor was evaluated by the ratio of the central line-averaged electron density (r = 0) to the edge one (r = 24cm) measured by HCN interferometer. The electron temperature gradient $|\nabla Te|$ was obtained from ECE measurement in the core region (r/a~ 0.4). When $|\nabla Te|$ are below 1.6 keV/m, the TEMs are not observed and the peaking factors are above 13. However, when $|\nabla Te|$ = 1.6keV/m is exceeded, the TEM is excited and the peaking factors decrease with the gradients. The TEM is enhanced with the increased temperature gradient. Since the particle convection velocity driven by TEM is radially outward [11, 17], the enhanced outward transport could reduce the inward particle flux and then decrease the peaking factor. The result suggests the contribution of TEM to the outward particle convection.

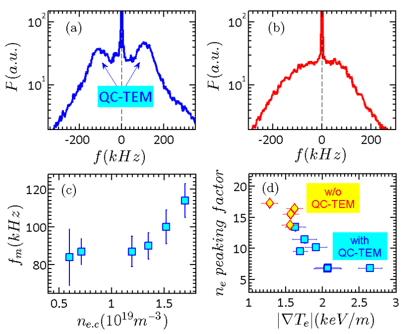

FIG. 13. Doppler spectrum (a) with and (b) without QC-TEM in J-TEXT plasmas, (c) characteristic frequency of QC-TEM versus cut-off density of two O-mode multi-channel Doppler reflectometers, (d) density peaking factor versus core electron temperature gradient for the plasmas with and without QC-TEM

4. Observations of Behavior of Runaway Current Due to RMPs

The effect of RMP with m/n=2/1 dominant component on runaway generation during disruptions has been investigated recently. The parameters of the target plasma are as follows:

B_t = 2.3 T, I_p = 180 kA, $\bar{n}_{e0}$ = 1.0×10^{19} m^{-3}. The fast valve is fired at 0.4 s with moderate argon injection to produce stable runaway current plateau. Owing the amplitude and duration of runaway plateau varied from shot to shot but with same plasma parameter and same argon injection, the effect of the 5 kA static RMPs ($\delta B/B_t$ = 1.3×10^{-4}) on runaway suppression can be performed statistically, as shown in Fig. 14. Both the amplitude and the duration of runaway current plateau decreased with the application of RMP.

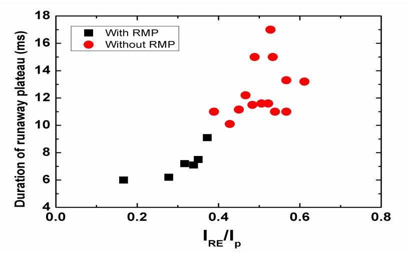

FIG. 14. Duration of runaway plateau vs fraction of runaway current with or without static RMPs.

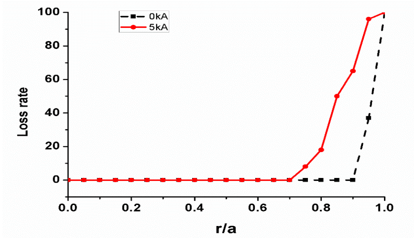

FIG. 15. The loss rate of runaway electrons launched on the different minor radius.

Based on Hamiltonian guiding center equations for runaway electrons, the effect of resonant magnetic perturbation (RMP) on the confinement of runaway electrons is simulated by calculating the orbit losses for different runaway initial energies and different runaway initial locations. The result indicates that the loss rate of runaway electrons is sensitive to the radial position of electrons as shown in Fig. 15. The simulation has shown that the loss of energetic runaway beam is dominated by the shrinkage of the confinement region. Outside the shrinkage region of runaway beam the runaways are lost rapidly. Inside the shrinkage region the runaway beam is confined very well and is less sensitive to the magnetic perturbation. This can explain the partial suppression of runaway current formation by RMP [42].

5. Conclusions

The application of RMPs to the J-TEXT plasma has extended the operating region. The experiments indicate that moderate amplitude of applied RMPs can increase the density limit and lower edge safety factor..

The plasma current shrinkage in the MARFE region during MARFEs is observed for the first time by using the 17-channel POLARIS. Such localized plasma current shrinkage would produce a strong radial magnetic field around the q = 2 surface, which is sufficient to trigger the 2/1 locked mode and cause the major disruption. The results offer a reasonable interpretation for the mechanism of MARFE and density limit disruptions.

The observations of an externally applied RMP with large 3/1 component on electron density show that the electron density first increases (decreases) inside (around/outside) of the 3/1 rational surface, and it is increased globally later together with enhanced edge recycling. The toroidal momentum transport is also studied using the perturbative analysis technique on J-TEXT. The results show that a pinch effect in the momentum transport exists during the electrode-biasing phase. The electrostatic turbulence exhibited quasi-coherent characteristics in the spectra of density fluctuations. The results indicate that the QCMs survive in the linear Ohmic confinement regime of the plasma, where the TEM is predicted to be unstable.

The Investigations of behaviors of r of runaway current by the applied RMPs indicate that the magnetic perturbation enhanced the runaway loss rate by the formation magnetic islands rather than by the magnetic perturbation itself. The experimental observations are also confirmed by the simulation results.

Acknowledgement This work is supported by the National Magnetic Confinement Fusion Science Program of China under Contract No. 2015GB111001 and 2015GB111002, and the National Natural Science Foundation under Contract No. 11505069.

References

[1] ZHUANG, G., et al., “The reconstruction and research progress of the TEXT-U tokamak in China ”, Nucl. Fusion **51**(2011) 094020.
[2] ZHUANG, G., et al., “Recent research work on the J-TEXT tokamak”, Nucl. Fusion **53**(2013) 104014.
[3] ZHUANG, G., et al., “Overview of the recent research on the J-TEXT tokamak”, Nucl. Fusion **55**(2015) 104003.
[4] FITZPATRICK, R., “Interaction of tearing modes with external structures in cylindrical geometry (plasma)”, Nucl. Fusion **33**(1993) 1049.
[5] FITZPATRICK, R., et al., “Improved evolution equations for magnetic island chains in toroidal pinch plasmas subject to externally applied resonant magnetic perturbations”, Physics of Plasmas **8**(2001) 4489.
[6] HU, Q., et al., “Effect of externally applied resonant magnetic perturbations on resistive tearing modes”, Nucl. Fusion **52**(2012) 083011.
[7] HU, Q., et al., “Understanding the effect of resonant magnetic perturbations on tearing mode dynamics”, Physics of Plasmas **20**(2013) 092502.
[8] LIPSCHULTZ, B., et al., “Marfe: an edge plasma phenomenon”, Nucl. Fusion **24**(1984) 977.
[9] LIPSCHULTZ, B., “Reviews of marfe phenomena in tokamaks”, Journal of Nuclear Materials **145**(1987) 15.
[10] RAPP, J., et al., “Operational limits under different wall conditions on TEXTOR-94”, Journal of Nuclear Materials **290-293**(2001) 1148.
[11] GARBET, X., et al., “Physics of transport in tokamaks”, Plasma Phys. Control. Fusion **46**(2004) B557.
[12] NORDMAN, H., et al., “Simulation of toroidal drift mode turbulence driven by temperature gradients and electron trapping”, Nucl. Fusion **30**(1990) 983.
[13] HOANG, G.T., et al., “Experimental Determination of Critical Threshold in Electron Transport on Tore Supra”, Phys. Rev. Lett. **87**(2001) 125001.
[14] MANTICA, P., et al., “Experimental Study of the Ion Critical-Gradient Length and Stiffness Level and the Impact of Rotation in the JET Tokamak”, Phys. Rev. Lett. **102**(2009) 175002.
[15] VILLEGAS, D., et al., “Experimental Electron Temperature Gradient Dependence of Heavy Impurity Transport in Fusion Devices”, Phys. Rev. Lett. **105**(2010) 035002.
[16] HILLESHEIM, J.C., et al., “Observation of a Critical Gradient Threshold for Electron Temperature Fluctuations in the DIII-D Tokamak”, Phys. Rev. Lett. **110**(2013) 045003.
[17] ZHONG, W.L., et al., “Convective Velocity Reversal Caused by Turbulence Transition in Tokamak Plasma”, Phys. Rev. Lett. **111**(2013) 265001.
[18] RICE, J.E., et al., “Rotation Reversal Bifurcation and Energy Confinement Saturation in Tokamak Ohmic L-Mode Plasmas”, Phys. Rev. Lett. **107**(2011) 265001.
[19] ARNICHAND, H., et al., “Quasi-coherent modes and electron-driven turbulence”, Nucl. Fusion **54**(2014) 123017.
[20] KRAMER-FLECKEN, A., et al., “Long-range correlation properties of quasi-coherent modes at TEXTOR”, New J. Phys. **17**(2014) 073007.
[21] SMITH, H.M., et al., “Hot tail runaway electron generation in tokamak disruptions”, Phys. Plasmas **15**(2008) 072502.

[22] YOSHINO, R., et al., “Fast plasma shutdown by killer pellet injection in JT-60U with reduced heat flux on the divertor plate and avoiding runaway electron generation”, Plasma Phys. Control. Fusion **39**(1997) 313.
[23] YOSHINO, R., et al., “Runaway electrons in magnetic turbulence and runaway current termination in tokamak discharges”, Nucl. Fusion **40**(2000) 1293.
[24] LEHNEN, M., et al., “Runaway generation during disruptions in JET and TEXTOR”, Journal of Nuclear Materials **390-391**(2009) 740.
[25] LEHNEN, M., et al., “Suppression of Runaway Electrons by Resonant Magnetic Perturbations in TEXTOR Disruptions”, Phys. Rev. Lett. **100**(2008) 255003.
[26] CHENG, Z.F., et al., “Edge impurity rotation profile measurement by using high-resolution ultraviolet/visible spectrometer on J-TEXT”, Rev. Sci. Instrum. **85**(2014) 11E423.
[27] ZHUANG, G., et al., “The three-wave laser polarimeter-interferometer on J-TEXT tokamak”, Journal of Intstrumentation **11**(2016) C02026.
[28] CHEN, J., et al., “High resolution polarimeter-interferometer system for fast equilibrium dynamics and MHD instability studies on Joint-TEXT tokamak (invited)”, Rev. Sci. Instrum. **85**(2014) 11D303.
[29] DRAKE, J.F., “Marfes: Radiative condensation in tokamak edge plasma”, Physics of Fluids **30**(1987) 2429.
[30] CHEN, X.P., et al., “Multifaceted asymmetric radiation from the edge: A strong condensation phenomenon”, Phys. of Plasmas **3**(1996) 4507.
[31] VAN NIEUWENHOVE, R., “Charge neutralization by poloidal plasma rotation”, Plasma Phys. Control. Fusion **34**(1992) 873.
[32] LIPSCHULTZ, B., “Ultrahigh Densities and Volume Recombination inside the Separatrix of the Alcator C-Mod Tokamak”, Phys. Rev. Lett. **81**(1998) 1007.
[33] CHEN, J., et al., “Equilibrium reconstruction based on core magnetic measurement and its applications on equilibrium transition in Joint-TEXT tokamak ”, Rev. Sci. Instrum. **85**(2014) 103501.
[34] HU, Q., et al., "Plasma response to m / n = 3/1 resonant magnetic perturbation at J-TEXT Tokamak", Nucl. Fusion **56** (2016) 092009
[35] HENDER, T.C., et al., “Effect of resonant magnetic perturbations on COMPASS-C tokamak discharges”, Nucl. Fusion **32**(1992) 2091.
[36] FRASSINETTI, L., et al., “The tearing mode locking–unlocking mechanism to an external resonant field in EXTRAP T2R”, Plasma Phys. Control. Fusion **56**(2014) 104001.
[37] SUN, Y., et al., “Investigations of turbulent transport and intrinsic torque of toroidal momentum at the edge of J-TEXT tokamak with electrode biasing”, Nucl. Fusion **56**(2016) 046006.
[38] LOPES CARDOZO, N.J., “Perturbative transport studies in fusion plasmas”, Plasma Phys. Control. Fusion **37**(1995) 799.
[39] JIN, W., et al., “Upgraded high time-resolved x-ray imaging crystal spectroscopy system for J-TEXT ohmic plasmas”, Rev. Sci. Instrum. **85**(2014) 023509.
[40] ZHONG, W.L., et al., “Spatiotemporal characterization of zonal flows with multi-channel correlation Doppler reflectometers in the HL-2A Tokamak”, Nucl. Fusion **55**(2015) 113005.
[41] ARNICHAND, H., et al., “Identification of trapped electron modes in frequency fluctuation spectra”, Plasma Phys. Control. Fusion **58**(2016) 014037.
[42] JIANG, Z.H., et al., “Simulation of runaway electrons, transport affected by J-TEXT resonant magnetic perturbation”, Nucl. Fusion **56**(2016) 092012.